Search for the standard model Higgs boson in $\mathrm{H} \to \mathrm{ZZ} \to \ell^+\ell^-\tau^+\tau^-$ decay channel with the CMS experiment at $\sqrt{s} = 7$ and 8 TeV

Simranjit Singh Chhibra(1)(2)(*) (on behalf of the CMS Collaboration)

(1) *Università degli Studi di Bari - Bari, Italy - 70125*
(2) *Istituto Nazionale di Fisica Nucleare - Sezione di Bari, Italy - 70125*

Summary. — A search for the standard model Higgs boson in the decay mode $\mathrm{H} \to \mathrm{ZZ} \to \ell^+\ell^-\tau^+\tau^-$ ($\ell = e, \mu$) is presented. The analysis uses the proton-proton collision data recorded by the CMS experiment at the LHC, corresponding to integrated luminosity of 5.1 fb^{-1} at $\sqrt{s} = 7$ TeV and 12.2 fb^{-1} at $\sqrt{s} = 8$ TeV. Both the hadronic and leptonic decays of τ are inspected. No evidence is found for a significant deviation from the standard model expectations anywhere in the ZZ mass range considered in this analysis. An upper limit at 95% confidence level is placed on product of the cross-section and decay branching ratio for the Higgs boson decaying with standard model like couplings, which excludes the cross-sections of about two to four times the expected values for the Higgs boson masses in the range of $190 < m_{\mathrm{H}} < 600$ GeV/c^2.

PACS 14.80.Bn – Standard Model Higgs boson.

1. – Introduction

The discovery of the signal compatible with the production of the standard model (SM) [1, 2, 3] Higgs boson would, in particular, shed light on the mechanism of spontaneous breaking of the electroweak symmetry [4, 5, 6, 7].

In July 2012, the CMS and ATLAS experiments announced the discovery of a new boson at a mass around 125 GeV [8, 9], with properties compatible with the SM Higgs boson. In his letter, a search for the SM Higgs boson in the decay mode $\mathrm{H} \to \mathrm{ZZ} \to \ell^+\ell^-\tau^+\tau^-$ ($\ell = e, \mu$) is presented, which is performed to set exclusion upper limits on the SM Higgs cross-section values for the mass range of $190 < m_{\mathrm{H}} < 1000$ GeV/c^2. This search complements the Higgs boson search in the $\mathrm{H} \to \mathrm{ZZ}^{(*)} \to 4\ell$ channel [10] at masses above the kinematical threshold for ZZ production. The presence of leptons in the final states provides a clean signature with small background contributions. The major sources of backgrounds are irreducible SM ZZ production, reducible Z and WZ production

(*) simranjit.chhibra@ba.infn.it

in association with jets, and $t\bar{t}$. In this analysis, both the Z bosons are required to be on-shell and the analysis covers the Higgs mass range of $190 < m_{\mathrm{H}} < 1000$ GeV/c^2. One Z, which is called 'leading', is required to decay into $\mu^+\mu^-$ or e^+e^- pair, whereas the second Z called 'sub-leading', decays into $\tau^+\tau^-$ pair with four possible final states: $\tau_h\tau_h$, $\tau_e\tau_h$, $\tau_\mu\tau_h$ and $\tau_e\tau_\mu$, where τ_h represents hadronically decaying taus, and τ_e, and τ_μ represents the taus decaying into electrons and muons respectively. The final states $\tau\tau \to \tau_e\tau_e, \tau_\mu\tau_\mu$ are not considered, as they are accounted for in the $\mathrm{H} \to \mathrm{ZZ}^{(*)} \to 4\ell$ Higgs search.

The analysis is based on data from proton-proton (pp) collisions at $\sqrt{s} = 7$ and 8 TeV, corresponding to integrated luminosity of 5.1 fb^{-1} and 12.2 fb^{-1} respectively, collected with the CMS experiment at the LHC in years 2011 and 2012 respectively.

2. – CMS Experiment

A detailed description of the CMS experiment can be found elsewhere [11]. The CMS uses a right-handed coordinate system, with the origin at the nominal interaction point, the x-axis is pointing to the centre of the LHC ring, the y-axis is pointing up (perpendicular to the LHC plane), and the z-axis is along the counterclockwise proton beam direction. The polar angle, θ, is measured from the positive z-axis and the azimuthal angle, ϕ, is measured in the x-y plane. Suppose the four-momentum of a particle has the coordinates (E, p_x, p_y, p_z), then the longitudinal component is given as p_z and the transverse component is given by $p_T = \sqrt{p_x^2 + p_y^2}$.

Particles produced in the pp collisions are detected in the pseudorapidity range of $|\eta| < 5$, where $\eta = -\ln[\tan(\theta/2)]$. The central feature of the CMS apparatus is a superconducting solenoid, of 6 m internal diameter, providing a uniform magnetic field of 3.8 T in the bore, equipped with silicon pixel and strip tracking systems ($|\eta| < 2.5$) surrounded by a lead tungstate crystal electromagnetic calorimeter (ECAL) and a brass-scintillator hadronic calorimeter (HCAL) covering $|\eta| < 3$. A steel/quartz-fiber Cherenkov calorimeter extends the coverage to $|\eta| < 5$. The steel return yoke outside the solenoid is instrumented with gas ionization detectors used to identify muons up to $|\eta| < 2.4$.

3. – Event Reconstruction

A complete reconstruction of the individual particles emerging from each collision event is obtained via a particle-flow (PF) technique [12]. In the PF approach, information from all sub-detectors is combined to reconstruct and identify particles produced in the collision. The particles are classified into mutually exclusive categories: charged hadrons, photons, neutral hadrons, muons, and electrons.

The electrons are reconstructed within the geometrical acceptance, $|\eta| < 2.5$, and for $p_T > 7$ GeV/c. The reconstruction combines the information from clusters of energy deposits in the ECAL and the trajectory in the inner tracker [13, 14]. Electron identification relies on a multivariate technique that combines observables sensitive to the amount of bremsstrahlung along the electron trajectory, the geometrical and momentum matching between the electron trajectory and associated clusters, as well as shower-shape observables [10].

Muons are reconstructed within $|\eta| < 2.4$ and with $p_T > 5$ GeV/c by using information from both the inner tracker and the muon spectrometer [15]. The PF muons are selected among the reconstructed muon track candidates by applying minimal requirements on

the track components in the muon system and taking into account the matching with small energy deposits in the calorimeters [16].

The PF particles are used to reconstruct hadronically decaying taus using the 'Hadron Plus Strip' (HPS) algorithm [17], which is designed to optimize the performance of τ_h reconstruction and identification by considering specific τ_h decay modes. The π^0 components of the τ_h are first reconstructed and then combined with charged hadrons to reconstruct the τ_h decay modes. The neutrinos produced in all taus decays escape detection and are ignored in the τ_h reconstruction. The algorithm provides high τ_h identification efficiency, approximately 50%, for the range of τ_h energies relevant for this analysis. The 'medium' and 'tight' isolation working points of HPS algorithm are used in this analysis. The τ_h in this analysis are required to have $|\eta| < 2.3$ and $p_T > 20$ GeV/c.

4. – Event Selection and Monte Carlo Samples

The events selected for this analysis pass the triggers which require the presence of at least two muons or electrons in the event satisfying minimum p_T threshold values. The threshold values varied for the different data taking periods due to the different instantaneous luminosities recorded by the CMS experiment. Two muons with minimum p_T threshold value of 7 GeV/c in the event were required for the particular event to satisfy the double muon trigger, in the starting period of pp collisions in year 2011. The p_T threshold values increased asymmetrically to 13 and 8 GeV/c for the leading and sub-leading muons respectively, in the middle period of year 2011, and to 17 and 8 GeV/c afterwards. The same p_T threshold value had been continued for data collection in year 2012. For the double electron events, the p_T threshold values of 17 and 8 GeV/c were used for leading and sub-leading electrons respectively, for years 2011 and 2012.

Events are required to have at least one leading Z candidate decaying into either a pair of oppositely charged electrons or muons with p_T greater than 20 GeV and 10 GeV for leading and sub-leading leptons, respectively. A mass window of 60–120 GeV/c^2 is set on the invariant mass of the leading Z which reduces the contribution of $t\bar{t}$ background since the mass distribution of di-lepton pairs produced in $t\bar{t}$ decays shows a non-resonant behavior. Both leptons are required to be isolated with PF combined relative isolation less than 0.25. The PF combined relative isolation in a cone of $\Delta R = \sqrt{\Delta\eta^2 + \Delta\phi^2} < 0.4$ around the lepton direction is defined as

$$I_{rel}^{PF}(\rho) = \frac{\sum \left(p_T^{charged} + max(0, E_T^{neutral} + E_T^{\gamma} - \rho \times A_{eff} \right)}{p_T^{\ell}} \tag{1a}$$

where $\sum p_T^{charged}$ is scalar sum of the transverse momenta of charged hadrons originating from the primary vertex. The primary vertex is chosen as the vertex with the highest sum of p_T^2 of its constituent tracks. The $\sum E_T^{neutral}$ and $\sum E_T^{\gamma}$ are the sum of transverse energies of the neutral hadrons and photons, respectively. The average transverse momentum flow density, ρ, is calculated in each event using a 'jet area' technique [28]. It is defined as the median of the distribution for the neutral particles around all jets (any PF jet in the event having $p_T^{jet} > 3$ GeV/c). The effective area, A_{eff}, is the geometric area of the isolation cone times a correction factor which accounts for residual dependence of the isolation on pile-up as a function of η.

For the sub-leading Z boson, a tau pair is selected. Since taus decay either leptonically or hadronically, if the final state contains only muons and electrons, the leptons are required to have p_T in excess of 10 GeV/c. Since τ_hs have a much larger misidentification rate than leptons, if one tau decays hadronically, the isolation on the electron and muon is required to be tighter (less than 0.15 for muon and 0.10 for electron). The τ_h is required to pass the medium isolation working point. For both taus decaying hadronically, they are required to pass the tight isolation working point.

A mass window of 30–90 GeV/c^2 is set on the visible invariant mass of the sub-leading Z if one or both the taus decay hadronically. An extended mass window of 0–90 GeV/c^2 is set if both taus decay leptonically. This avoids the contribution of sub-leading $Z \to 2\ell$ where the muons or electrons are misidentified as τ_hs. At the last step of selection, an overlap check for the selected events and $H \to ZZ \to 4\ell$ events is performed since there is high probability of the lepton(s) coming from the sub-leading Z decays to be misidentified as τ_h(s). This check rejects the event if in addition to the four objects, another electron or muon with $p_T > 10$ GeV/c and $I_{rel}^{PF} < 0.4$, or a τ_h passing the loose isolation working point is found in the event.

The event yields are found in good agreement with the MC background expectations at each step of the event selection.

A set of Monte Carlo (MC) event samples is used to simulate signal and background events. The Drell-Yan background, $\ell^+\ell^-$ in association with jets, is simulated with the MC generator MadGraph [18], with cross-sections rescaled to next-to-next-to-leading order (NNLO) prediction for inclusive Z production. The SM background contribution from ZZ production via $q\bar{q}$ is generated at next-to-leading order (NLO) with POWHEG [19]. The $gg \to$ ZZ contribution is generated with gg2ZZ [20]. The di-boson WZ background is simulated with MadGraph. The $t\bar{t}$ samples are simulated at NLO with POWHEG. The tau decays are generated with TAUOLA [21]. The Higgs boson signals from gluon-fusion ($gg \to H$), and vector-boson fusion ($qq \to qqH$), are generated with POWHEG at NLO. All events are processed through a detailed simulation of the CMS detector based on GEANT4 [22] and reconstructed with the same algorithms that are used for data.

5. – Background Estimates and Systematic Uncertainties

The ZZ estimate is based on the MC prediction. One the other hand, a data-driven approach, so-called Fake Rate (FR) method, is used to estimate the reducible backgrounds since they occur due to the presence of jets that can be misidentified as τ_hs, electrons and muons. The jet to τ_h FR defined as the probability of τ_hs to be isolated, is measured using events in which the leading Z passes all selection requirements and di-τ_h pairs are observed, where τ_hs are required to have the same charge. This region is dominated by $Z + jets$ events with signal contamination of less than 0.1%. The FR is measured for medium and tight isolation working points. The measured FR is then fit with a function of the hadronic tau p_T given as

$$F(p_T(\tau_h)) = C_0 + C_1 e^{C_2 p_T(\tau_h)} \tag{2a}$$

The measured FR parametrized in the hadronic tau p_T for both isolation working points along with the fit results are given in fig. (1) for 2011 data. A comparison of FR measurements from data and MC is also given. Both measurements are found in good agreement above the hadronic tau p_T threshold of 20 GeV/c, used in this analysis.

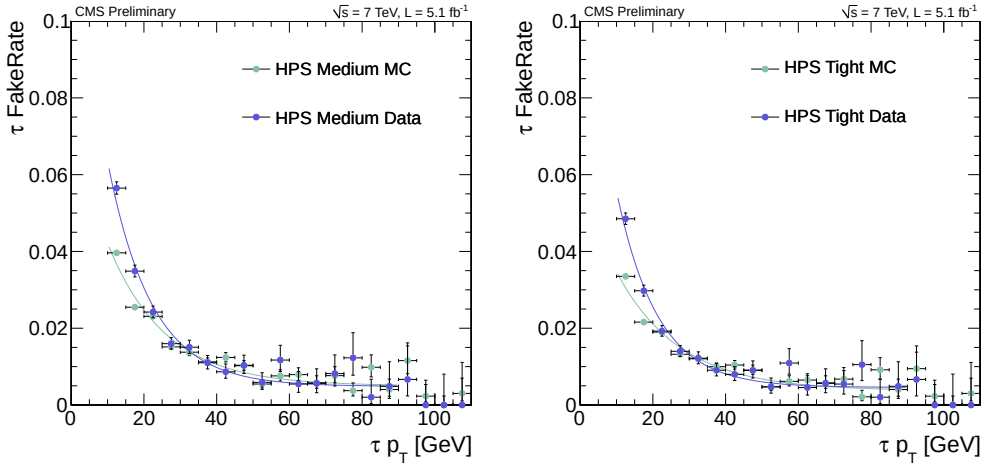

Fig. 1.: Data to MC comparison for jet to τ_h FR as a function of hadronic tau p_T for the medium (left) and tight (right) isolation working points with the resulting fit overlaid, for 2011 data.

Te similar procedure is applied to measure the jet to electron(muon) FR using events with leading Z passes all selection requirements and $\tau_{e(\mu)}\tau_h$ pairs are observed with zero net charge.

To estimate the number of background events in the signal region, the measured FR is applied to events which pass all selection requirements, including proper charge combination of the sub-leading Z. The events are divided into three categories: both objects coming from sub-leading Z decays are anti-isolated, *cat*1, one object is isolated and second object is anti-isolated, *cat*2, and vise-versa of second category, *cat*3. The *cat*1 is dominated by $\mathrm{Z} + jets$ events and on the other hand, $\mathrm{WZ} + jets$ events give a dominant contribution in the later two categories. The final estimation by taking into account the contamination of *cat*1 events in *cat*2 and 3 if one object gets misidentified, is given by

$$\begin{aligned} N^{est}_{reducible} &= N_0 \times F_1 \times F_2 + (N_1 - N_0 \times F_2) \times F_1 + (N_2 - N_0 \times F_1) \times F_2 \\ &= N_1 \times F_1 + N_2 \times F_2 - N_0 \times F_1 \times F_2 \end{aligned} \tag{3a}$$

where N_0, N_1 and N_2 are the number of events in *cat*0, 1 and 2 respectively. The F_1 and F_2 are the measured FR for first and second objects respectively.

Theoretical uncertainties on the Higgs boson cross-section for whole mass range (17–20%) and branching ratio (2%) are taken from ref. [23]. The current searches for a heavy Higgs boson at LHC assume the on-shell (stable) Higgs boson production, describing the Higgs lineshape with a Breit-Wigner distribution. This approximation breaks down at high Higgs boson mass (typically > 400 GeV/c^2) due to the very large Higgs width (> 70 GeV/c^2). The lineshape is therefore corrected to match the results presented in refs. [24, 25] using a more correct approach to describe the Higgs mass distribution, known as Complex Pole Scheme (CPS). The main uncertainty on the estimate of ZZ background arises from the theoretical uncertainty on the ZZ production cross-section and

is taken from ref. [26]. The total uncertainty on the the reducible background estimate which comes from uncertainties on the measured FR values and the limited statistics of the control regions in the data, is approximately 30%. The uncertainty on integrated luminosity of the data sample is 2.2% at $\sqrt{s} = 7$ TeV and 4.4% at $\sqrt{s} = 8$ TeV [27]. Systematic uncertainties on trigger efficiency (1.5%) and on lepton identification and isolation efficiencies are evaluated from data. The uncertainties associated with lepton identification and isolation efficiencies are 1–2% for muons and electrons, and 6% for τ_h. Uncertainties on τ_h energy scales (3%) contribute to variation in the shape of the mass spectrum.

6. – Results

Forty five $\ell^+\ell^-\tau^+\tau^-$ candidate events have been observed in 2011 and 2012 data, corresponding to integrated luminosity of 5.1 fb^{-1} at $\sqrt{s} = 7$ TeV and 12.2 fb^{-1} at $\sqrt{s} = 8$ TeV respectively, and 19.0±2.3, and 20.4±6.2 background events are expected in total for ZZ and reducible backgrounds. The expected events for Higgs boson signal of mass 200 GeV/c^2 are 5.6 ± 0.6 summing over all the final states. Fig. (2) reports an event display of $ee\tau_e\tau_h$ candidate event observed in 2012 data, in the CMS experiment. The event candidate consists of three well isolated electrons with tracks (light blue) in the tracker system and the energy deposits in the calorimeter system. The τ_h is represented with green track and deposits energy in HCAL. The solid red arrow represents the direction of missing transverse energy. The missing p_T vector is computed as the opposite of the p_T sum of all PF particles reconstructed in the event and the magnitude of this vector gives the missing transverse energy. The $\ell^+\ell^-\tau^+\tau^-$ visible invariant mass is shown in fig. (3) for the combination of 2011 and 2012 analysis.

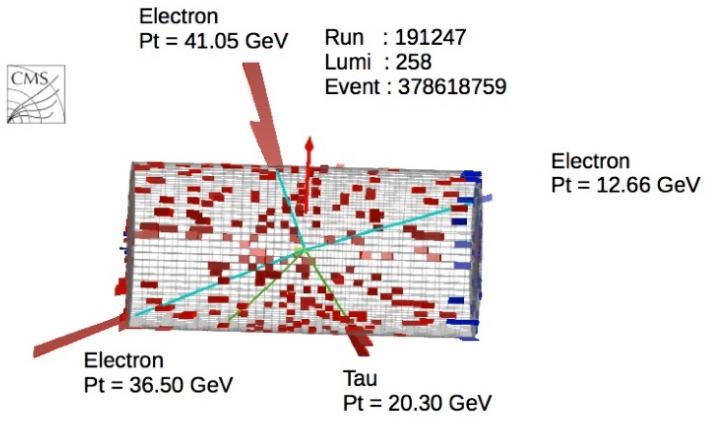

Fig. 2.: Event display for $ee\tau_e\tau_h$ candidate event in 2012 data.

Expected and observed 95% confidence level (CL) upper limits are set on the ratio of the production cross-section to the nominal SM Higgs cross-section using the CLs method [28, 29] by taking all the sources of systematic uncertainties into account. They are presented as a function of the Higgs mass in fig. (3). No evidence is found for a

significant deviation from the SM expectations anywhere in the Higgs boson mass range considered in this analysis. The differences between the observed and expected limits are found consistent with statistical fluctuations and the observed limits reside within 68% band of the expected one. The upper limit of two to four times the SM expectations has been observed for Higgs mass range of $190 < m_{\mathrm{H}} < 600$ GeV/c^2.

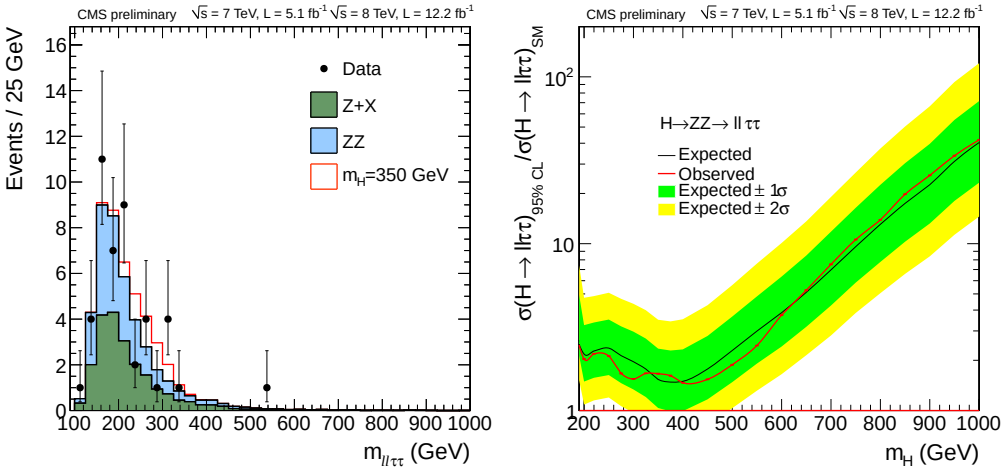

Fig. 3.: Distribution of the $\ell^+\ell^-\tau^+\tau^-$ reconstructed mass in full mass range for the sum over all final states (left). Points represent the data, shaded histograms represent the background and unshaded histogram represent the signal expectations for Higgs boson mass of 350 GeV/c^2. The background shapes are taken from MC simulation and are normalized to the values obtained using control data samples, as described in the text. Observed and expected 95% CL upper limits (right) on the ratio of the production cross-section to the SM expectation. The 68% and 95% ranges of expectation for the background-only model are also shown with green and yellow bands, respectively.

* * *

I congratulate my colleagues in the CERN accelerator departments for the excellent performance of the LHC machine.

REFERENCES

[1] Glashow S. L., *Nucl. Phys.*, **22** (1961) 579.
[2] Weinberg S., *Phys. Rev. Lett.*, **19** (1967) 1264.
[3] Salam A., *Elementary particle physics: relativistic groups and analyticity*, **N. Svartholm, ed., p. 367. Almquvist & Wiskell** (1968) Proceedings of the eighth Nobel symposium.
[4] Englert A. and Brout R., *Phys. Rev. Lett.*, **13** (1964) 321.
[5] Higgs P.W., *Phys. Lett.*, **12** (1964) 132;**Phys. Rev. Lett.** (13) 1964508;**Phys. Rev.** (145) 19661156.
[6] Guralnik G. and Hagen C. and Kibble T., *Phys. Rev. Lett.*, **13** (1964) 585.
[7] Kibble T., *Phys. Rev. Lett.*, **155** (1967) 1554.
[8] CMS Collaboration, *Phys. Lett. B*, **716** (2012) 30-61.
[9] ATLAS Collaboration, *Phys. Lett. B*, **716** (2012) 1-29.

[10] CMS Collaboration, *CMS Phys. Ana. Sum.*, **HIG-12-041** (2012) .
[11] CMS Collaboration, *JINST*, **3** (2008) S08004.
[12] CMS Collaboration, *CMS Phys. Ana. Sum.*, **CMS-PAS-PFT-09-001** (2009) .
[13] Baffioni S. et al., *Eur. Phys. J. C*, **49** (2007) 1099.
[14] CMS Collaboration, *CMS Phys. Ana. Sum.*, **CMS-PAS-EGM-10-004** (2010) .
[15] CMS Collaboration, *JINST*, **7** (2012) P10002.
[16] CMS Collaboration, *CMS Phys. Ana. Sum.*, **CMS-PAS-PFT-10-003** (2010) .
[17] CMS Collaboration, *JINST*, **7** (2012) P10001.
[18] Alwall J. et al., *JHEP*, **09** (2007) 028.
[19] Frixione S. and Nason P. and Oleari C., *JHEP*, **11** (2007) 070.
[20] Binoth T. and Kauer N. and Mertsch P., *arXiv:0807.0024*, **doi:10.3360/dis.2008.142.** (2008) Proceedings of the XVI Int. Workshop on Deep-Inelastic Scattering and Related Topics (DIS'07).
[21] Jadach S. et al., *Comput. Phys. Commun.*, **76** (1993) 361.
[22] Allison J. et al., *Nucl. Sci.*, **53** (2006) 270.
[23] LHC Higgs Cross Section Working Group, *CERN Report*, **CERN-2011-002** (2011) .
[24] Passarino G. and Sturm C. and Uccirati S., *Nucl. Phys. B*, **834** (2010) 77.
[25] Goria S. and Passarino G. and Rosco D., *Nucl. Phys. B*, **864** (2012) 530-579.
[26] LHC Higgs Cross Section Working Group, *CERN Report*, **CERN-2012-002** (2012) .
[27] Lai H.L. et al., *Phys. Rev. D*, **82** (2010) 074024.
[28] Junk T., *Nucl. Instrum. Meth. A*, **434** (1999) 435.
[29] Read A.L., *CERN Report*, **CERN-OPEN-2000-005** (2000) .